

Characteristics and variability of synoptic features associated with cool season rainfall in southeastern Australia

James S. Risbey,^{a*} Michael J. Pook,^a Peter C. McIntosh,^a Caroline C. Ummenhofer,^b and Gary Meyers^c

^a *The Centre for Australian Weather and Climate Research, Hobart, Australia*

^b *Climate Change Research Centre, University of NSW, Sydney, Australia*

^c *University of Tasmania, Hobart, Australia*

ABSTRACT: Cool season rainfall variability in southeastern Australia is investigated via classification and characterization of the predominant types of synoptic systems occurring in the region. These types are frontal systems, cut-off low systems, and other systems. Rainfall in the region is dominated by cut-off systems and these systems are the main influence on the interannual variability of rainfall. Both cut-off systems and frontal systems display an enhancement of thermal (thickness) gradient as rainfall increases, but the mechanisms for intensification differ. Cut-off systems intensify in the region in association with local increases in baroclinicity and the subtropical jet, whereas frontal systems tend to intensify via a confluence of subtropical and polar jets. Interannual rainfall variability is examined for groupings of years based on both clustering of continental rainfall patterns and on El Niño/Southern Oscillation (ENSO)/Indian Ocean Dipole (IOD) years. Cut-off systems exhibit consistent enhancements of thermal gradients for groupings of years in which they produce more rainfall. For ENSO/IOD groupings, the cut-off thermal gradients are consistent with the underlying sea surface temperature (SST) anomalies. Wet years in southeastern Australia are usually produced by cut-off systems, but can also be produced by frontal systems. In those cases the mid-tropospheric flow pattern is reminiscent of the negative Southern Annular Mode (SAM) pattern. The positive SAM pattern is also associated with enhanced rainfall in the southeast via local intensification of blocking and cut-off systems. Copyright © 2008 Royal Meteorological Society

KEY WORDS synoptic climatology; climate variability; rainfall variability; extratropical cyclone

Received 10 September 2007; Revised 19 June 2008; Accepted 21 September 2008

1. Introduction

Southeastern Australia undergoes significant interannual and decadal rainfall variability and is currently in the midst of an extended period of drought (Gallant *et al.*, 2007; Watkins and Trewin, 2007). The variability of agricultural production in the region is closely related to the variability of rainfall (Nicholls, 1997). Rainfed agriculture in southeastern Australia (grains, sheep, and other livestock) is sensitive to year-to-year fluctuations in rainfall, while irrigated agriculture in the region (fruit, viticulture, dairy) is more sensitive to longer period (decadal) fluctuations in rainfall.

Southeastern Australia is one of the most productive agricultural regions in Australia, though its output varies dramatically in wet and dry seasons in rainfed sectors. The gross domestic product of the rural areas of southeast Australia drops by about 20% in major drought years (Adams *et al.*, 2002). The sources of rainfall variability in the region are thus of interest to the agricultural

producers. In this paper, we document some of the processes associated with rainfall variability in southeastern Australia. In particular, we describe the synoptic features associated with major rainfall events and rainfall variability using a broad set of dynamical diagnostics. We also relate rainfall variability to the major modes of seasonal and interannual variability in the proximate oceans.

The climate of southeastern Australia follows a general Mediterranean pattern, with warm, dry summers, and cooler, wetter winters. The seasonal cycle of rainfall in the region displays a moderate peak in the winter months. Winter rainfall tends to be dominated by mid-latitude storm systems, though interaction with tropical features and moisture sources is often important in the development of these systems over Australia (McIntosh *et al.*, 2007). The amount of rainfall is strongly moderated by the location relative to the coast and to the Great Dividing Range (a mountain range skirting the east and southeast edge of the continent – see Figure 1). Locations inland of the Great Dividing Range receive much less rainfall than locations on the coastal side of the divide.

One of the major grain growing regions of Australia is located inland of the Dividing Range in southeastern Australia. This region relies in particular on rainfall through the cool season (April–October). Grain yields in

*Correspondence to: James S. Risbey, The Centre for Australian Weather and Climate Research, CSIRO Marine and Atmospheric Research, GPO Box 1538 Hobart, 7001 Australia.
E-mail: james.risbey@csiro.au

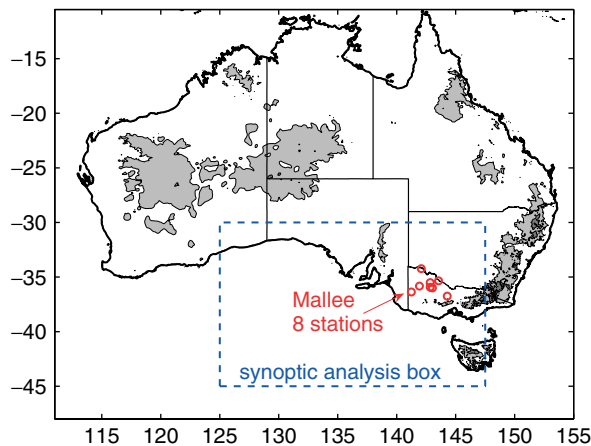


Figure 1. Map of Australia showing the locations of the synoptic analysis box and the Mallee rainfall stations. The synoptic box spans latitudes 30–45°S and longitudes 125–147.5°E. Areas of topography over 500 m are shaded, highlighting the Great Dividing Range in the southeast of the continent. This figure is available in colour online at www.interscience.wiley.com/ijoc

the region undergo large fluctuations in association with interannual variations in rainfall. We seek to diagnose and explain some of the sources of that variation. The approach we take is to characterize the different synoptic systems that produce rainfall in this region, and to relate those systems in turn to broader scale features of the circulation.

The analysis of rainfall here is focused on the ‘Mallee’ region, which is a part of the inland region described above. The Mallee region is shown in Figure 1. The selection of this subregion provides a smaller area that is more homogeneous than the broader southeast from the point of view of any given synoptic storm system. By choosing a smaller region, we can be surer that rainfall across the region is the result of the same storm at roughly the same point in the storm’s life-cycle. Though there can be large variations in rainfall across the region for any given storm, rainfall is still fairly highly correlated on this scale and it is reasonable to average stations in the region to produce a Mallee rainfall average.

The paper is organized as follows. In the next section we describe the features of rainfall in the Mallee region.

Then we describe the major cool season synoptic types and a scheme for classifying them. We then analyse how rainfall is associated with each synoptic type and how the synoptic types vary in wet and dry years in the region. Since much of the interannual variability in rainfall in the region is governed by variations in ocean and atmospheric states in the Pacific and Indian Oceans, we also analyse the modulation of rainfall and synoptic types by the El Niño/Southern Oscillation (ENSO) (Philander, 1985) and Indian Ocean Dipole (IOD) (Saji *et al.*, 1999) states in the penultimate sections.

2. Mallee rainfall

Rainfall in the Mallee region is represented here by the average of rain over eight stations across the Mallee region. The eight stations are Bendigo, Birchip, Kaniva, Mildura, Narraport, Rainbow, Sea Lake, and Swan Hill. The station locations are indicated by circles in Figure 1. These stations are all part of the Bureau of Meteorology high quality Australian historical dataset (Lavery *et al.*, 1997). Any gaps in the Bureau of Meteorology records have been filled with interpolated data from the Queensland Department of Natural Resources and Mines patch point dataset (Jeffrey *et al.*, 2001). A full description of the eight-station data is provided in Pook *et al.* (2006).

For the dataset spanning the period 1889–2006, the mean annual rainfall for the eight-station average is 380 mm, with a standard deviation of 100 mm. A time series of the annual rainfall is shown in Figure 2. At least three extended drought periods are apparent in the record, centred around 1900, 1940, and the present period. There is little or no apparent trend in rainfall over the full period of record.

Annual rainfall amounts for the Mallee are dominated by contributions from daily rainfall in the range from 2–10 mm/day. The time series of annual rainfall as a function of daily rainfall amount is shown in Figure 3. During wetter years the annual rainfall has larger than normal contributions from daily totals in the range to about 15 mm/day, while dryer periods and years are marked by an absence of contributions from daily totals in this range. The higher rainfall events are important

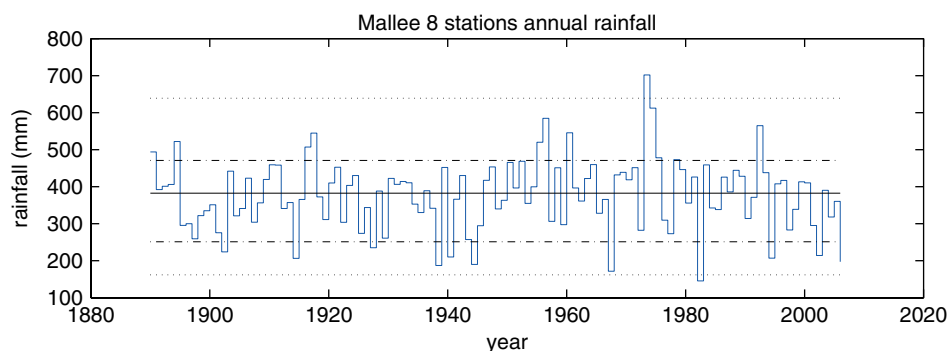


Figure 2. Time series of Mallee eight station annual rainfall (stepped line). The solid line indicates the median rainfall, the dash-dot lines show the 10th and 90th percentile rainfall values, and the dotted lines show the 1st and 99th percentiles. This figure is available in colour online at www.interscience.wiley.com/ijoc

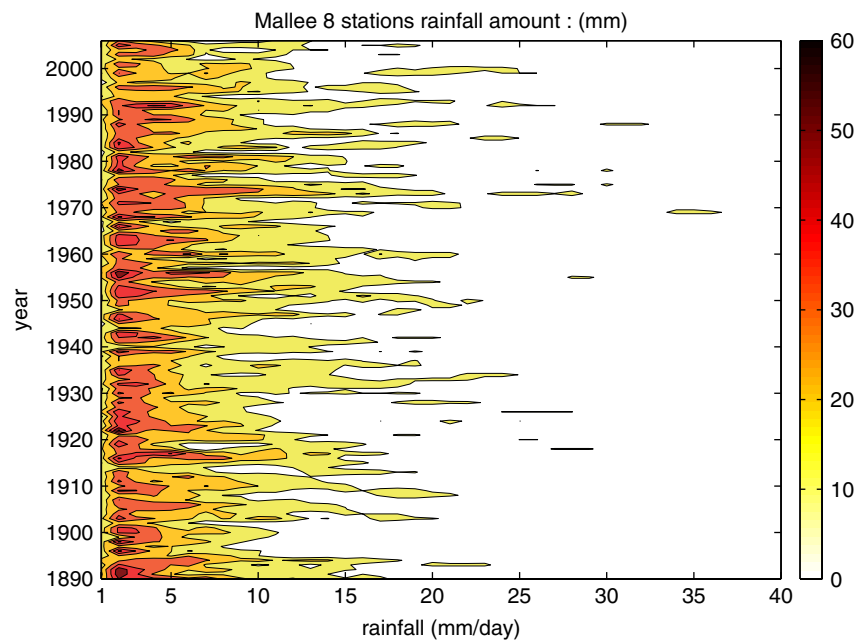


Figure 3. Hovmoller time series of Mallee eight station annual rainfall (in mm) as a function of the amount of rainfall per rainfall intensity category. The rainfall intensity categories are calculated from daily rainfall for bins of width 1 mm. The results have been smoothed across bins to facilitate interpretation in the Hovmoller plot. The contoured values show the amount of rain that fell each year in each rain intensity category. These amounts are calculated from the number of events in each category times the amount of rain in the category. This figure is available in colour online at www.interscience.wiley.com/ijoc

because they underpin variability in the record, and because they tend to provide more useful contributions to crop growth. Rainfall events in the low end of the range (1–5 mm/day) are less useful because the moisture is more readily evaporated and does not penetrate the soil (McIntosh *et al.*, 2007). Owing to the fact that interannual variability of rainfall and the utility of rainfall are linked to rainfall intensities, it is important to diagnose which synoptic systems produce higher rainfall events. This issue is taken up in Section 3.

The seasonal cycle of rainfall in the Mallee is dominated by rainfall in the cool season period of April–October, which is nearly twice that which falls in the warm season months. Rainfed grain agriculture in the region follows the cool season maximum, with planting dates around the beginning of this period and harvest dates toward the end of the period. In order to match our analysis with the cool season cropping cycle, we focus on rainfall in the period of April through October in the analysis which follows.

3. Synoptic classification and data

Cool season rainfall in the Mallee region of southeastern Australia is produced by synoptic systems which generally traverse the westerly belt of the southern oceans and the Australian continent. In order to classify the rain-bearing systems in this region Pook *et al.* (2006) defined an analysis box centred on and west of the Mallee region. The location of the box is shown in Figure 1.

We used the synoptic classification of Pook *et al.* (2006) to classify synoptic events. This scheme classifies

each day on which rain occurs in the Mallee according to three basic synoptic types. These types are ‘cold-frontal systems of all types, cold-cored lows that have become cut-off from the westerly airstream (cut-off lows), and a combined category designated “others”, which includes particular airstream types, waves in the easterlies, and open troughs aloft’ (Pook *et al.*, 2006, p1162). Cut-off low systems are defined by Pook *et al.* as those where either (1) a closed low is present at 500 hPa with an associated cold trough evident in the 1000–500 hPa thickness field (marked by a negative thickness anomaly of at least 20 gpm); or (2) a closed low is present in the mean sea level pressure (mslp) field (< 1008 hPa) with an associated cold trough aloft with a negative thickness anomaly of at least 20 gpm. The definitions of frontal systems and cut-off systems employed follow conventional understanding in the literature. A detailed description of each synoptic type is provided in Pook *et al.* (2006).

For the cool season (April–October), cut-off lows account for about half the total rainfall in the Mallee region, frontal systems account for about a third of the total, and other systems account for the remainder (Pook *et al.*, 2006). The interannual variability of cool season Mallee rainfall is dominated by variability in contributions from cut-offs, both because they are the dominant source, and because their rainfall is more variable from year-to-year than that due to frontal systems (Pook *et al.*, 2006). Further, cut-offs contribute more of the heavier rainfall events, which are generally more useful for crop growth (McIntosh *et al.*, 2007). If we are to gain a better understanding of rainfall variability, then we need to

understand which systems generate the rainfall and what drives variability in these systems. A first step in this process is to diagnose and describe these systems. In Section 4 we analyse the structure of each synoptic type in the Australian region.

In order to characterize each synoptic type, we have utilized data from the National Centers for Environmental Prediction [(NCEP)/NCAR] reanalysis over the period 1970–2005 (Kalnay *et al.*, 1996). The reanalysis provides 6-hourly analyses at the standard atmospheric levels on a $2.5^\circ \times 2.5^\circ$ grid. The period since 1970 is generally well-characterized in the reanalysis over the Australian region because the upper air network is well developed by then and the satellite coverage has commenced (Bromwich and Fogt, 2004).

For each synoptic type, we analyse its thermal signature, measures of its development, and steering of the flow pattern using diagnostics derived from the reanalysis data. For a measure of the thermal signature, we use the 1000–500 hPa thickness anomaly, Z_A . The anomalies are calculated relative to the climatological mean for each location, (x, y) , at the relevant time, t :

$$Z_{Ax,y,t} = Z_{500x,y,t} - Z_{1000x,y,t} - \overline{Z_{500x,y} - Z_{1000x,y}} \quad (1)$$

where the overbar indicates a climatological mean ($\frac{1}{n} \sum_{t=1}^n Z_{x,y,t}$).

One measure of development of the systems is provided by the Eady growth rate. This index assesses baroclinic instability through the vertical gradient in horizontal wind in the middle troposphere (Hoskins and Valdez, 1990). The Eady growth rate, σ_{BI} , at a grid point is calculated from:

$$\sigma_{BI} = 0.31 \frac{f}{N} \left| \frac{\partial \mathbf{v}}{\partial z} \right| \quad (2)$$

where f is the Coriolis parameter, N is the Brunt-Väisälä frequency, z is vertical distance, and \mathbf{v} is the horizontal wind vector at 400 and 600 hPa (Paciorek *et al.*, 2002). The seasonal mean Eady growth rate is shown for the Australian region in Figure 4. The Eady growth rate displays a maximum over the east coast of Australia in winter and a secondary maximum at high

latitudes. These maxima follow the regions of subtropical and polar jet maxima. In summer, the maximum in Eady growth rate moves south of the continent as the summer jet moves south.

In order to assess system development, we also calculate the relative vorticity, ζ , for each system:

$$\zeta = \frac{\partial v}{\partial x} - \frac{\partial u}{\partial y} + \frac{u}{a} \tan(\phi) \quad (3)$$

where u and v are zonal and meridional wind components, x and y are zonal and meridional distance, a is the radius of the Earth, and ϕ is latitude. For the southern hemisphere, regions of large negative relative vorticity are indicative of cyclonic storms. The advection of vorticity into an unstable region of the atmosphere is thought to be important for the development of storm systems (Petterssen, 1955). We calculate relative vorticity at 500 hPa to provide an indication of vorticity in the middle troposphere. The seasonal mean relative vorticity for winter and summer over the Australian region is shown in Figure 5. In winter there is a broad band of cyclonic vorticity across the southern part of the continent, with a maximum off the east coast in the Pacific Ocean. There is a local maximum of anticyclonic vorticity in the Tasman Sea south of Tasmania and New Zealand, which is indicative of a tendency for blocking there (Trenberth and Mo, 1985).

Another measure of development is provided by consideration of the location of the system relative to the proximate jet stream. The jet stream also provides an indication of the steering of the flow and system. We represent the jet stream here by the magnitude of the wind vector at 250 hPa, which is a typical level for the jet core. The seasonal mean jet stream for winter and summer over the Australian region is shown in Figure 6. In the winter mean pattern, there is a jet spanning the Australian continent with a core centred off the east coast in the Pacific, and split flow in the Tasman Sea. In summer the mean jet core has retreated well south of the Australian continent in Australian longitudes. The jet patterns help explain the seasonal mean relative vorticity patterns shown in Figure 5. For example, the shear and curvature

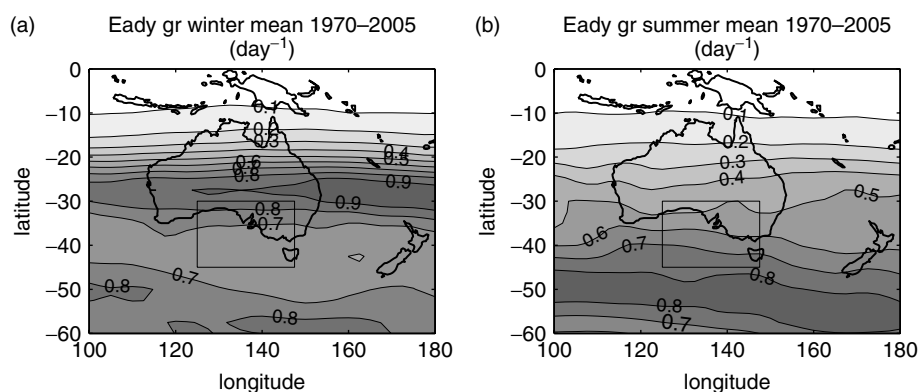


Figure 4. Seasonal mean Eady growth rate. Units are in day^{-1} . (a) represents winter (JJA) and (b) is for summer (DJF). The rectangular box shown here and on subsequent figures is the synoptic analysis box defined in Figure 1.

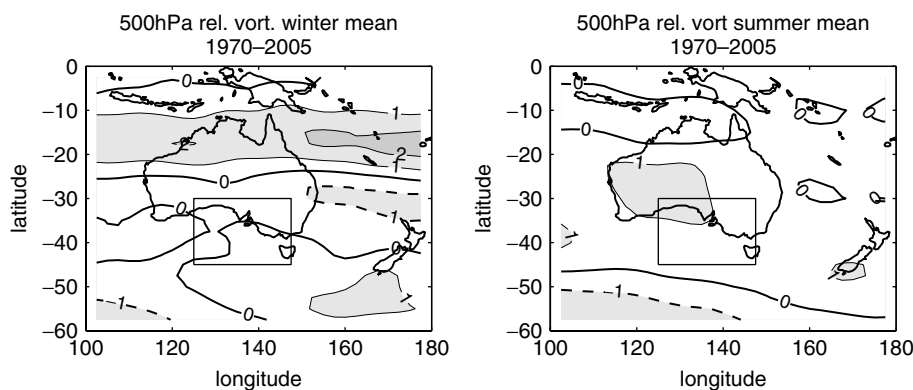


Figure 5. Seasonal mean 500 hPa relative vorticity. Units are in 10^{-5} s^{-1} . The left panel is for winter (JJA) and the right panel is for summer (DJF). Negative values (dashed contours) indicate cyclonic vorticity.

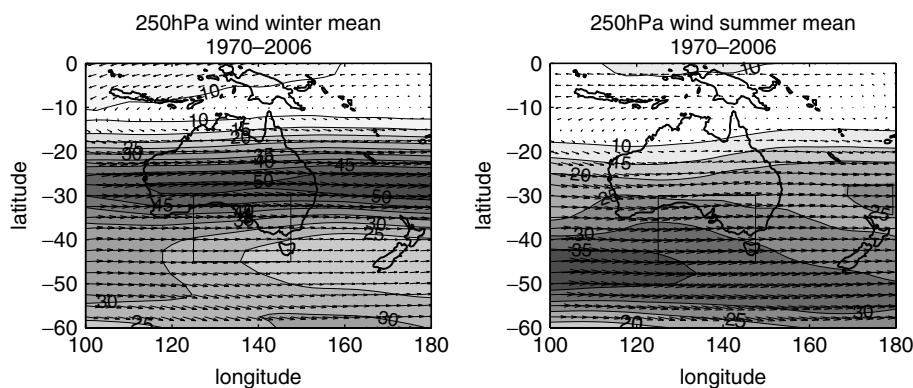


Figure 6. Seasonal mean 250 hPa wind. Units are in m s^{-1} . The left panel is for winter (JJA) and the right panel is for summer (DJF).

vorticity implied from the jet pattern in winter would predict the winter relative vorticity pattern with a band of anticyclonic vorticity north of the jet stream, a band of cyclonic vorticity south of the jet stream, and a region of anticyclonic vorticity in the Tasman Sea marking the region of split flow in the jet.

The final index used here to characterize a feature of the synoptic systems is vertical velocity, ω . Vertical velocity provides a further gross measure of instability and helps complete a view of the three-dimensional structure of the systems. Upward vertical velocities are a virtual prerequisite for rainfall. The rain layer in typical synoptic systems may extend over a wide range from the surface to the middle and upper troposphere for convective systems. We have selected 700 hPa to display the vertical velocity as this level is close to the middle of the rain layer for typical systems and will be within the rain layer in most systems. The seasonal mean vertical velocities (defined here as the negative of ω) over Australia are shown in Figure 7. These plots indicate Australia's location under regions of mean descent (negative vertical velocities) in the subtropical ridge. In summer, a monsoonal heat low is established in the northern part of the continent, giving rise to mean ascent there. Regions of mean ascent in midlatitudes are more salient near Australia in winter than summer.

Taken together, the winter mean indicators for Eady growth rate, relative vorticity, jet stream, and vertical

velocity shown in Figures 4, 5, 6 and 7 are not particularly propitious for winter rainfall in the Mallee region. In the winter mean fields, the Eady growth rate (Figure 4) and relative vorticity (Figure 5) both show maxima well downstream of the Mallee region, off the east coast of Australia. Thus, the main baroclinic zone and cyclonic vorticity regions, which are two critical ingredients for development, are more favorable for storminess in the Pacific than over southeastern Australia. Indeed, the winter mean vertical velocity field (Figure 7) shows downward motion over southeastern Australia, with upward motion off the east coast. Rainfall in the Mallee region is thus dependent on reorganizations and perturbations to the mean field provided by variation in broadscale circulation and the passage of synoptic systems. In the following section, we turn to analyses of the synoptic systems that provide these favorable perturbations.

4. Daily rainfall and synoptic types

In this section, we analyse the signature of each synoptic type according to the diagnostics described above. For each rainfall day in the Mallee region between April 1 and October 31 over the period 1970–2005, the synoptic type has been identified according to the criteria in Section 3. We have composited each of the fields above (thickness anomaly, Eady growth rate, relative vorticity, jet stream, and vertical velocity) over days with the

same synoptic type (cut-offs, fronts, other). We performed this compositing for the extended April–October cool season, and for overlapping 3-monthly seasons (AMJ, JJA, ASO). The overlap in seasons was used because the synoptic classification does not include months outside April–October. The results for the winter season (JJA) are generally typical of the various periods and are shown here.

In each case, we are interested in how the gross atmospheric structure varies according to the type of synoptic system. Further, we are also interested in how the structure varies according to the amount of rainfall that the

system produces. Thus, we have also further stratified the composites according to the intensity of rainfall. Rainfall days have been classified as weak (0.1–5 mm), moderate (5–15 mm), and heavy (>15 mm).

4.1. Thickness anomaly

Composites of thickness anomaly for cut-offs and fronts are shown in Figures 8 and 9 respectively. In each case there are marked warm (positive anomaly) and cold (negative anomaly) pools associated with the synoptic systems. The difference is that the cold pools for cut-off systems are cut-off from the westerlies by a warm

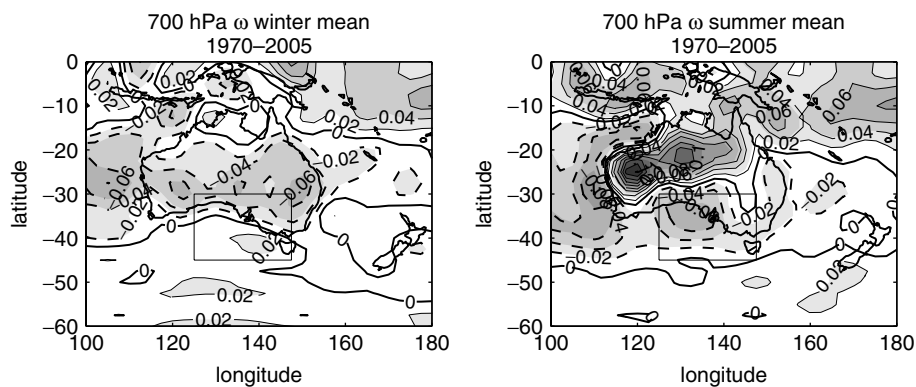


Figure 7. Seasonal mean vertical velocity at 700 hPa. Units are in Pa s^{-1} . Negative values (dashed contours) indicate descent. Positive values (solid contours) indicate ascent. The zero contour is bold.

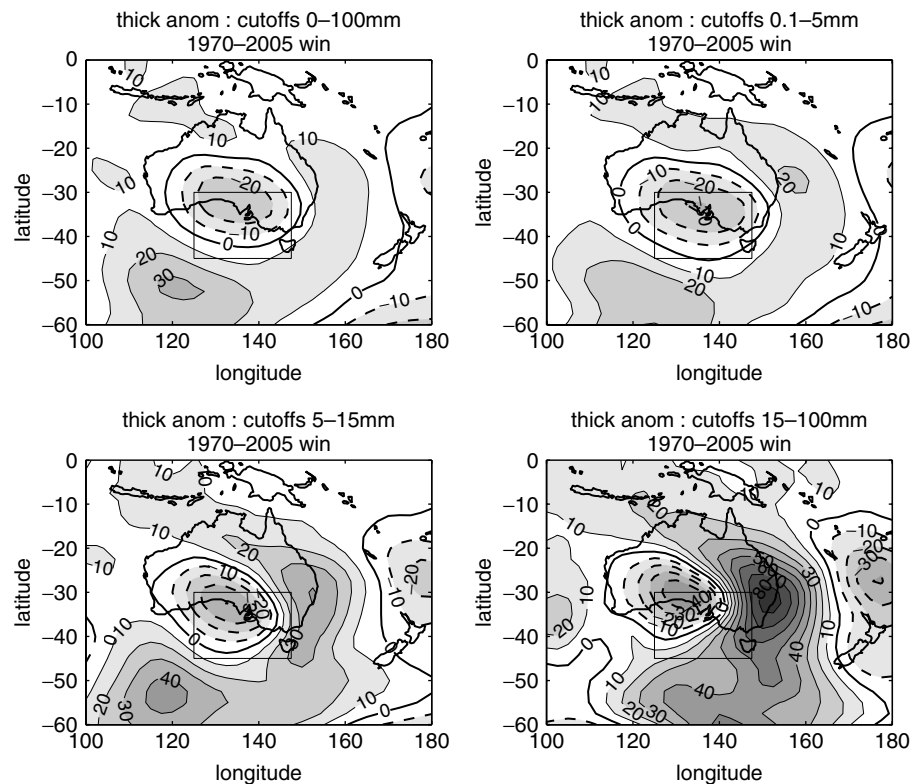


Figure 8. Composite of thickness anomaly for cut-off systems that accompany rain days in winters 1970–2005. The top left panel is a composite over all such rain days. The top right panel is a composite over just the subset of rain days that total less than 5 mm. The bottom left is for rain days between 5 and 15 mm, and the bottom right is for rain days greater than 15 mm. Units are in m. The box indicates the synoptic analysis region, as in Figure 1. Dash contours indicate negative anomalies and solid contours indicate positive anomalies.

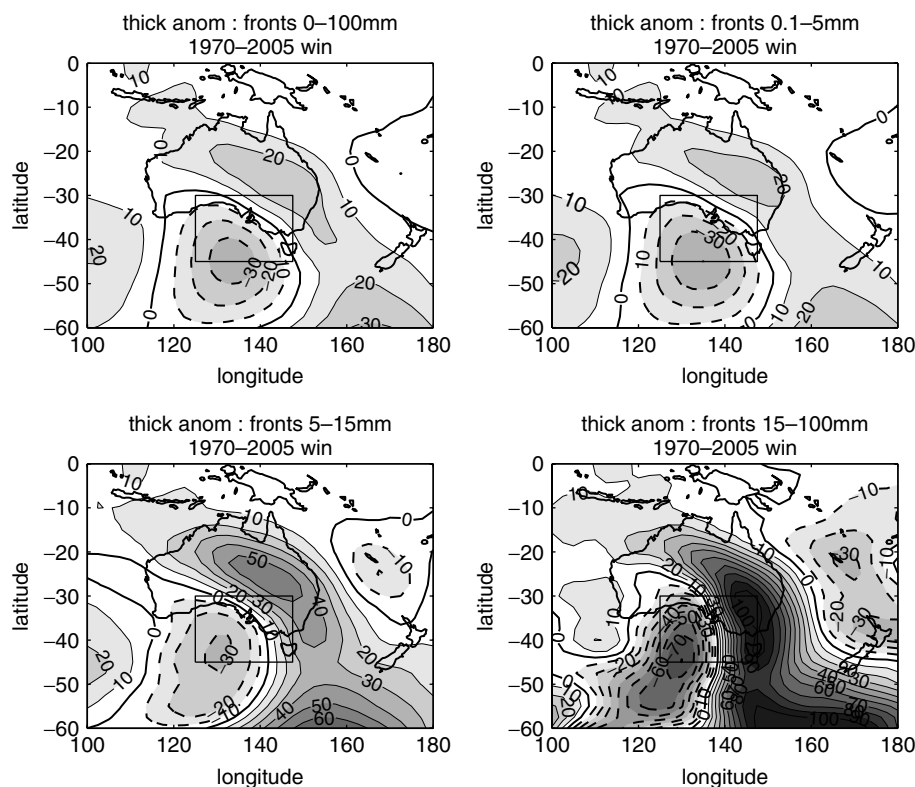


Figure 9. As in Figure 8, but for composites of thickness anomaly for frontal systems. Units are in m.

anomaly to the south which wraps around the cold anomaly, whereas for fronts the cold pool is contiguous with the westerly belt in the southern oceans.

As the amount of rain increases, the main change in Figures 8 and 9 is that the gradient of thickness anomaly across the synoptic system increases. This gradient increases primarily due to an increase in the magnitude of the warm anomaly. The cold anomaly increases in magnitude too, but not to the same degree. The increase in warm anomaly reflects stronger warm air advection ahead of the system, which is characteristic of developing systems (Hirschberg and Fritsch, 1991). The large warm anomaly produces an enhanced thickness gradient across the system, which is a feature of more highly developed systems (Sutcliffe and Forsdyke, 1950) and is thus consistent with the higher rainfall rates. The orientation of thickness anomaly gradients, with enhanced thickness to the northeast of the system centre and decreased thickness southwest, would lead to increases in thermal wind directed toward the southeast along the thickness gradient. The enhancement of thermal wind here would produce an acceleration of the jet stream in the vicinity of the system, promoting further development.

4.2. Eady growth rate

The Eady growth rate marks areas of favorable baroclinic development for storm systems. The composites of Eady growth rate for cut-offs are shown in Figure 10. The composites of Eady growth rate are compiled for the day prior to the rain event because the storm tends to develop in response to high values of Eady growth rate with a lag

of a day or so. For cut-off systems associated with weak rainfall events the pattern of Eady growth rate resembles the climatological mean pattern, following the major jets. For the heavy rainfall events the area of instability is increasingly concentrated over the analysis region. The pattern for frontal systems (not shown) is similar to that for cut-off systems, but the areal concentration of Eady growth rate is less pronounced for heavier rainfall events. Cut-off systems in the region are associated with, or promote, more concentrated values of Eady growth rate than frontal systems, which would be one factor behind their higher rainfall rates. In frontal systems, the highest values of Eady growth rate occur in the vicinity of the parent cyclone, which is well south of the synoptic box analysis region. Another factor promoting growth of the systems is the relative vorticity, which is discussed in the next section.

4.3. Relative vorticity

The relative vorticity for cut-off and frontal systems is shown in Figures 11 and 12 respectively. For cut-off systems (Figure 11), the maximum in cyclonic vorticity at the centre of the system intensifies as rainfall from the system increases. The cyclonic vorticity maximum is cradled to the south and southeast by a region of enhanced anticyclonic vorticity, which marks the blocking high associated with the cut-off low. This blocking high also intensifies as rainfall from the cut-off low increases. For frontal systems (Figure 12), the relative vorticity maximum also increases as rainfall from the system increases, but the maximum in cyclonic vorticity is

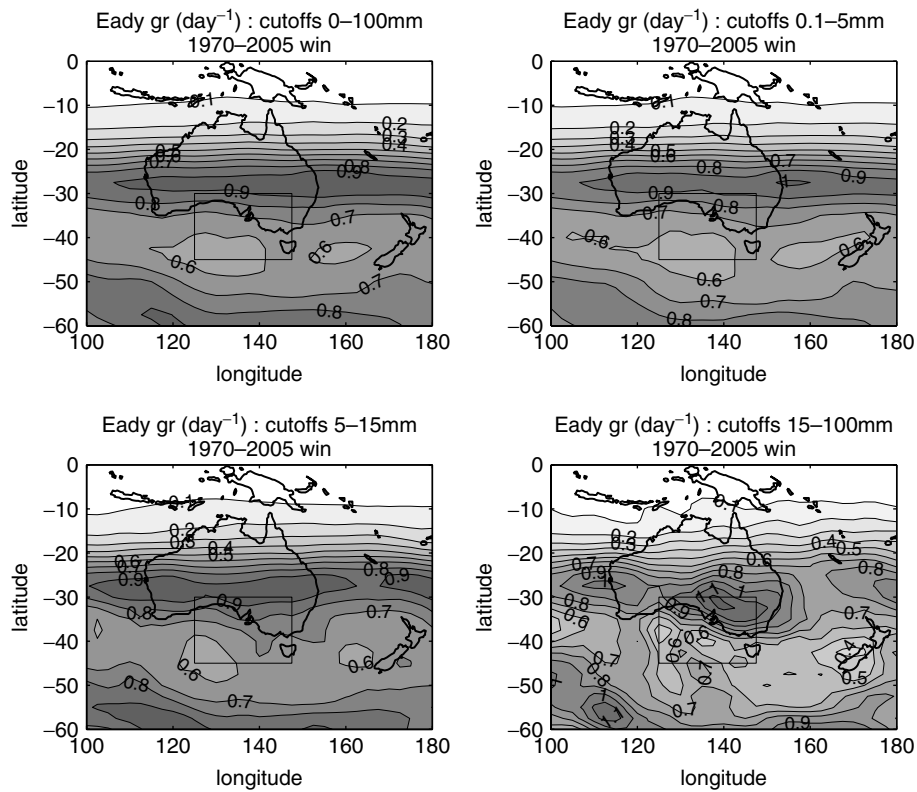


Figure 10. As in Figure 8, but for composites of Eady growth rate for cut-off systems. Units are in day^{-1} .

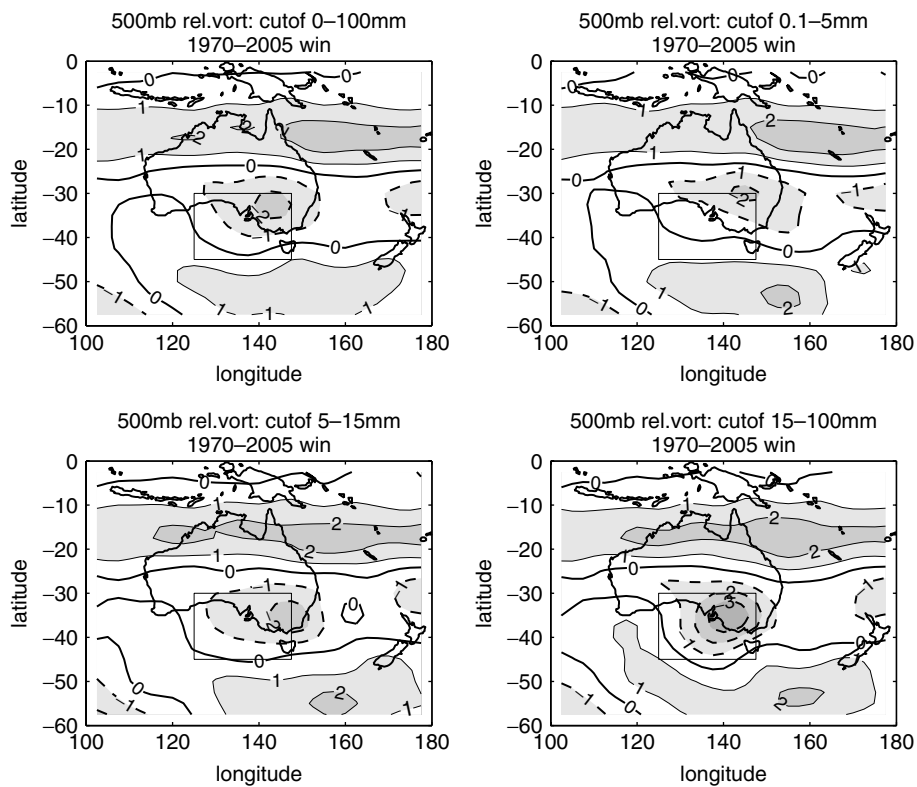


Figure 11. As in Figure 8, but for composites of relative vorticity for cut-off systems. Units are in 10^{-5} s^{-1} . Negative contours (dashed) indicate cyclonic vorticity.

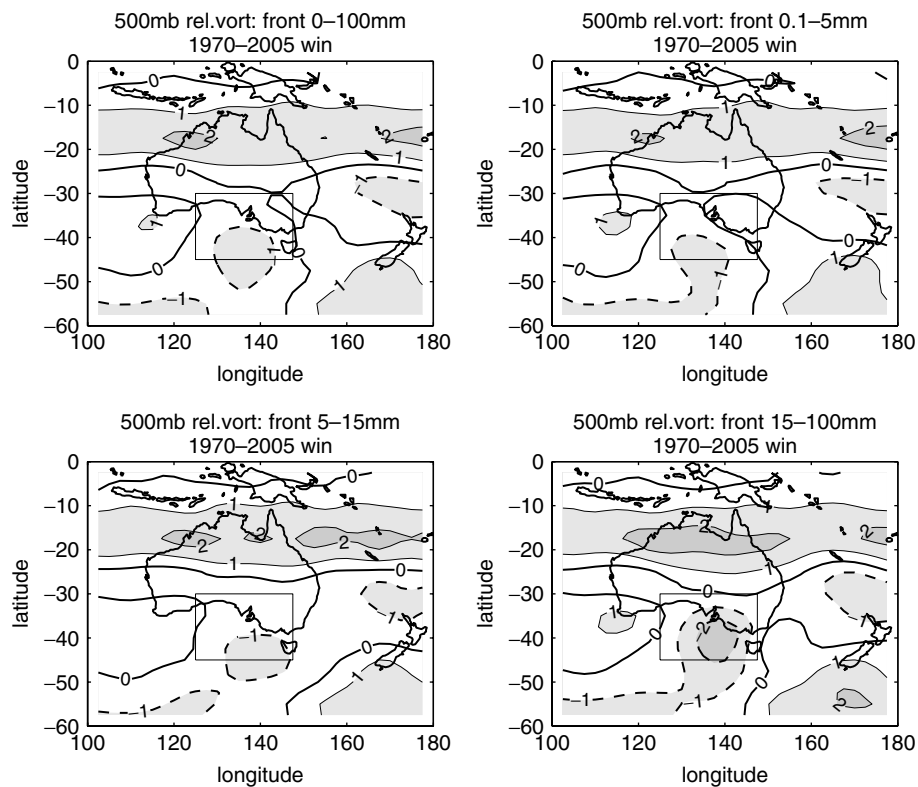


Figure 12. As in Figure 8, but for composites of relative vorticity for frontal systems. Units are in 10^{-5} s^{-1} .

weaker and located further south. The cyclonic vorticity maximum extends into the southern ocean in association with the influence of the polar front jet, which extends through this region in the more intense frontal systems (as shown in the next section).

The regions of cyclonic vorticity for cut-off (and front) composites are broadly coincident with the maxima in Eady growth rate indicated in Figure 10. However, the cyclonic vorticity maxima are more strongly localized about the synoptic system than the Eady growth rate maxima. Both Eady growth rate and relative vorticity fields display concentrated maxima in the synoptic box region for the most intense systems. The superposition of baroclinic zone and upper level vorticity displayed here is characteristic of the form of cyclonic development described by Petterssen (1955). The systems intensify as an upper level trough moves over a region of strong low level baroclinicity.

4.4. Jet streams

The signatures of the jetstream composites for cut-offs and fronts are quite different and are shown in Figures 13 and 14 respectively. For cut-off events (Figure 13), the subtropical jet is pronounced over the Australian continent and distinct from any branches of the polar jet. Cut-off systems are associated with the subtropical jet. As rainfall increases the subtropical jet is increasingly localized over the synoptic analysis region, with rainfall in the favorable 'right exit' region of the jet. This region of the jet is characterized by upper level

divergence and generates upward motion (Barry and Carleton, 2001), as is evident from the vertical velocity field in Figure 15. In addition, the baroclinic growth rates are highest in this region (Figure 10) and thickness anomaly gradients indicate an enhancement of the thermal wind (Figure 8). As the amount of rainfall associated with cut-offs increases, the cyclonic curvature of the jet also increases in Figure 13. This curvature tends to enhance the divergence and upmotion on the 'exit' side of the jet (Keyser and Shapiro, 1986), thus contributing to the development of the system and higher rainfall rates consistent with the other diagnostics.

In frontal systems (Figure 14), the polar jet merges with the subtropical jet in the vicinity of the frontal system. As the intensity of the rainfall event increases, the branch of the polar jet becomes more distinct, linking up directly with the subtropical jet to enhance the jet in the vicinity of the frontal system. Intense frontal systems in the region thus appear to gain energy via meridional excursions of the polar jet, while intense cut-off systems appear to gain energy from a localization and concentration of the subtropical jet. Like cut-off systems, intense frontal systems also show strong upward vertical velocities (Figure 16) in the right exit region of the jet (Figure 14). The increase in upward velocity also occurs in conjunction with strong warm advection. For frontal systems, cyclonic curvature of the jet core is evident only for the largest rainfall events in Figure 14. The features of the broader vertical velocity field and the factors which set it are discussed in the next section.

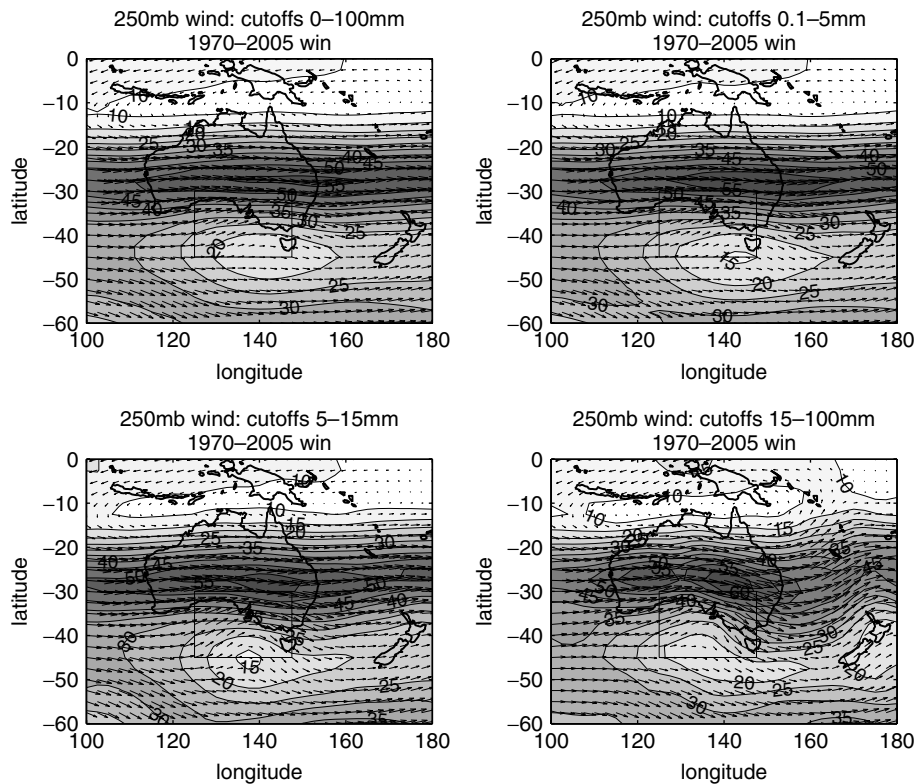


Figure 13. As in Figure 8, but for composites of 250 hPa wind for cut-off systems. Units are in m s^{-1} .

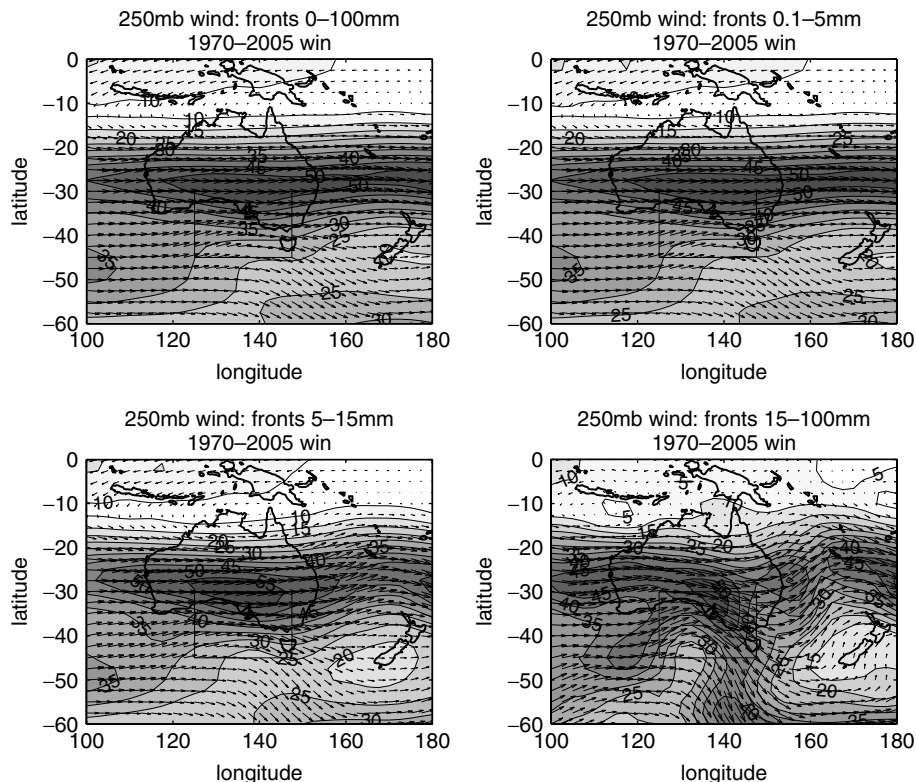


Figure 14. As in Figure 8, but for composites of 250 hPa wind for frontal systems. Units are in m s^{-1} .

4.5. Vertical velocity

Patterns of vertical velocity across storm systems help complete a view of the three-dimensional flow structure. Figures 15 and 16 show composites of the vertical

velocity field for cut-offs and fronts respectively. For both cut-offs and fronts there is a region of pronounced descent behind the system and a region of pronounced ascent ahead of the system. The areas of ascent occur in

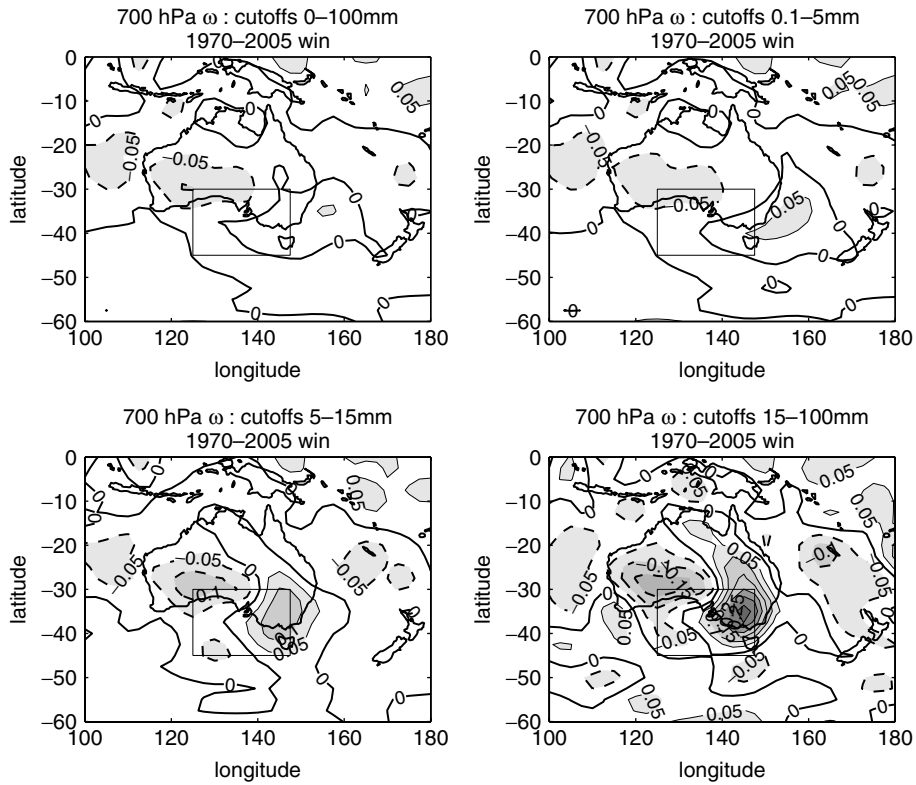


Figure 15. As in Figure 8, but for composites of vertical velocity for cut-off systems. Units are in Pa s^{-1} . Dash contours indicate descent and solid contours indicate ascent.

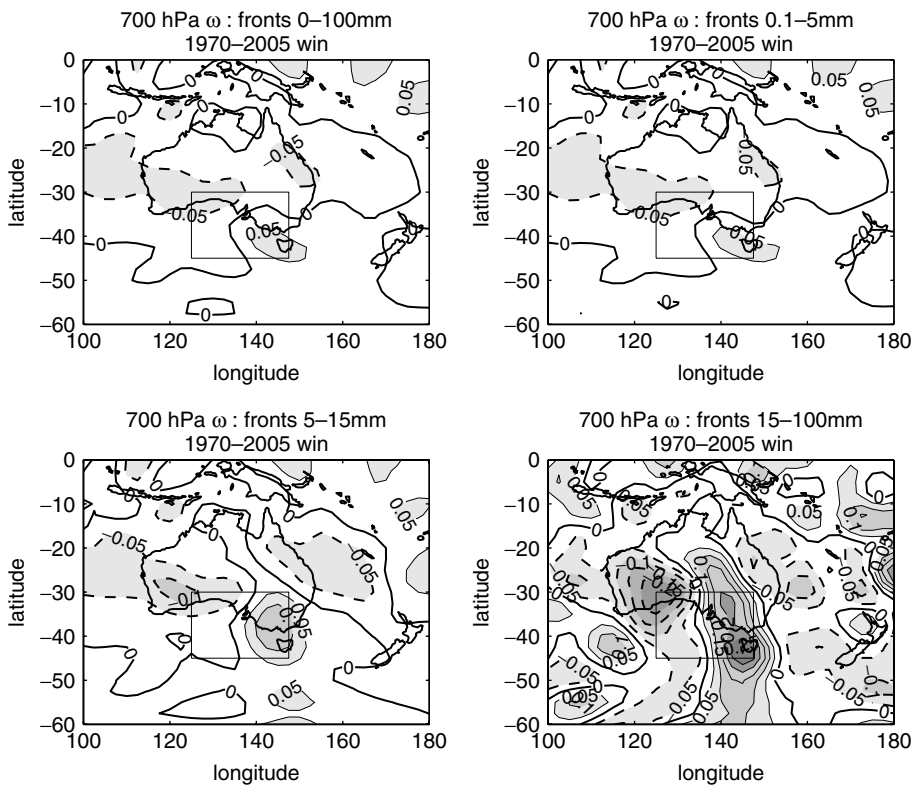


Figure 16. As in Figure 8, but for composites of vertical velocity for frontal systems. Units are in Pa s^{-1} .

the regions where warm advection is strongest (indicated by large positive thickness anomalies in Figures 8 and 9) and areas of descent occur in the regions where cold advection is strongest (indicated by large negative thickness anomalies in Figures 8 and 9) following expectations from quasi-geostrophic theory. The regions of ascent and descent increase in magnitude with increases in rainfall intensity of the systems. For cut-off systems the regions of descent and ascent tend to wrap around one another in classical 'comma' form, indicative of warm moist ascent ahead of the system and cold descent behind the system [e.g. Thorncroft *et al.* (1993); Griffiths *et al.* (1998)]. This feature is also enhanced as rainfall increases. For frontal systems, the region of ascent is more broadly aligned along a meridional band, consistent with the influence and orientation of the polar front jet (Figure 14).

5. Interannual rainfall

In the previous section, we investigated the variation in synoptic system structure as a function of rainfall intensity using daily rainfall data. In this section, we move to the interannual time scale. We start with large scale rainfall patterns on the seasonal scale and investigate whether there are coherent variations in synoptic structure that accompany these patterns. To construct seasonal rainfall patterns we have used gridded rainfall data for Australia spanning the period 1960–2004 (Jeffrey *et al.*,

2001). A clustering algorithm (Ward, 1963; Cheng and Wallace, 1993) was employed to identify five dominant patterns of rainfall across the Australian continent. These patterns for the winter season are shown in Figure 17. The patterns correspond to wetter than average conditions across the Great Dividing Range (wet Divide), wet across the southern part of the continent (wet south), wet along the east and west coasts (wet east/west coasts), dry over much of the continent (dry Australia), and wet over much of the continent (wet Australia), respectively. In the Mallee region, the high rainfall years correspond to the 'wet south' and 'wet Australia' patterns. The break up of rainfall by synoptic type for each of these rainfall patterns is shown in Figure 18. Winter rainfall in the Mallee region in the 'wet south' pattern is unusual in that it is dominated by fronts, whereas cut-offs dominate for most other patterns. In particular, the 'wet Australia' pattern is heavily dominated by rainfall from cut-off events.

The thickness anomalies that accompany each of these patterns are shown for cut-off systems in Figure 19 and frontal systems in Figure 20. For rainfall patterns in Figure 19 with higher than normal cut-off rainfall ('wet Divide' and 'wet Australia'), the cold thickness anomaly is particularly pronounced. For the much wetter 'wet Australia' pattern, the positive thickness anomaly off the east coast is also very pronounced, resulting in a strong thickness gradient. For patterns in Figure 20 where frontal rainfall is enhanced ('wet south' and 'wet Australia'), the gradient of thickness anomaly is also

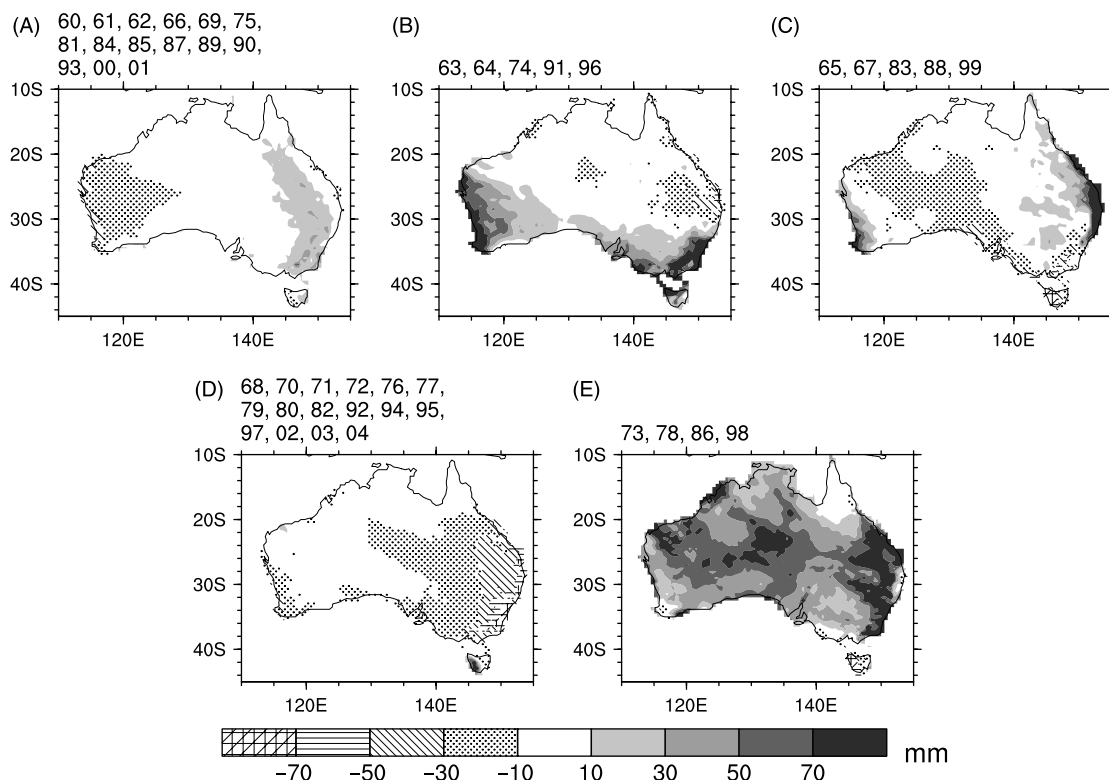


Figure 17. Winter rainfall anomaly patterns derived from a pattern cluster algorithm. The patterns are based on winter rainfall from the years 1960–2004. The years comprising each pattern are listed above the pattern. The shorthand descriptor for each pattern given in the text is 'wet Divide' (A), 'wet south' (B), 'wet east/west coasts' (C), 'dry Australia' (D), and 'wet Australia' (E), respectively. All shaded areas indicate statistically significant anomalies at the 80% level.

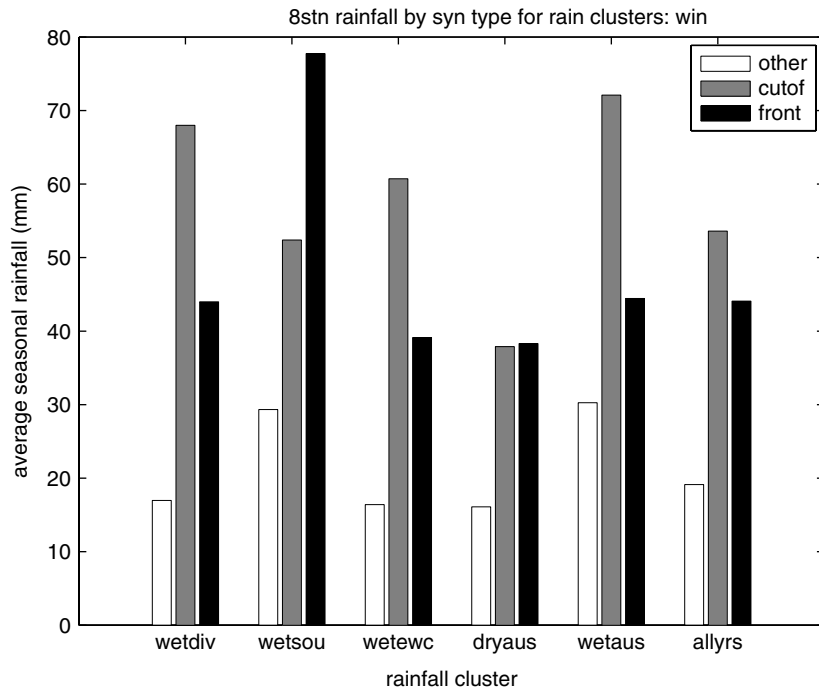


Figure 18. Mallee eight station rainfall by synoptic type for the rainfall cluster categories identified in Figure 17. The rainfall amounts plotted are the average winter rainfalls over the years in each rainfall cluster. The shorthand labels given correspond to the ‘wet Divide’, ‘wet south’, ‘wet east/west coasts’, ‘dry Australia’, and ‘wet Australia’ patterns respectively, and to all years.

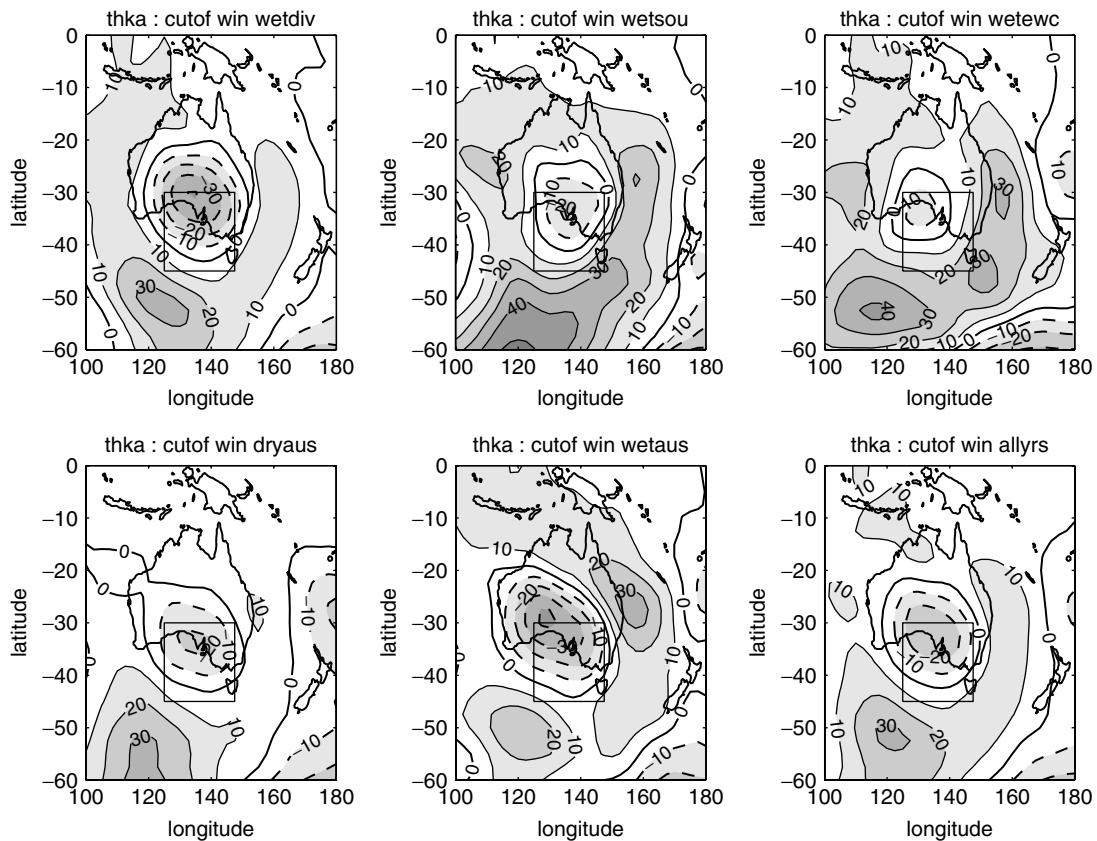


Figure 19. Thickness anomaly for the five rainfall cluster patterns shown in Figure 17 for winter days on which cut-off lows occur in each set of cluster years. The six panels correspond to the five patterns (Wet Divide, Wet south, Wet east/west coast, Dry Australia, Wet Australia) and to all years (1960–2004). Units are in m. Dash contours indicate negative anomalies and solid contours indicate positive anomalies.

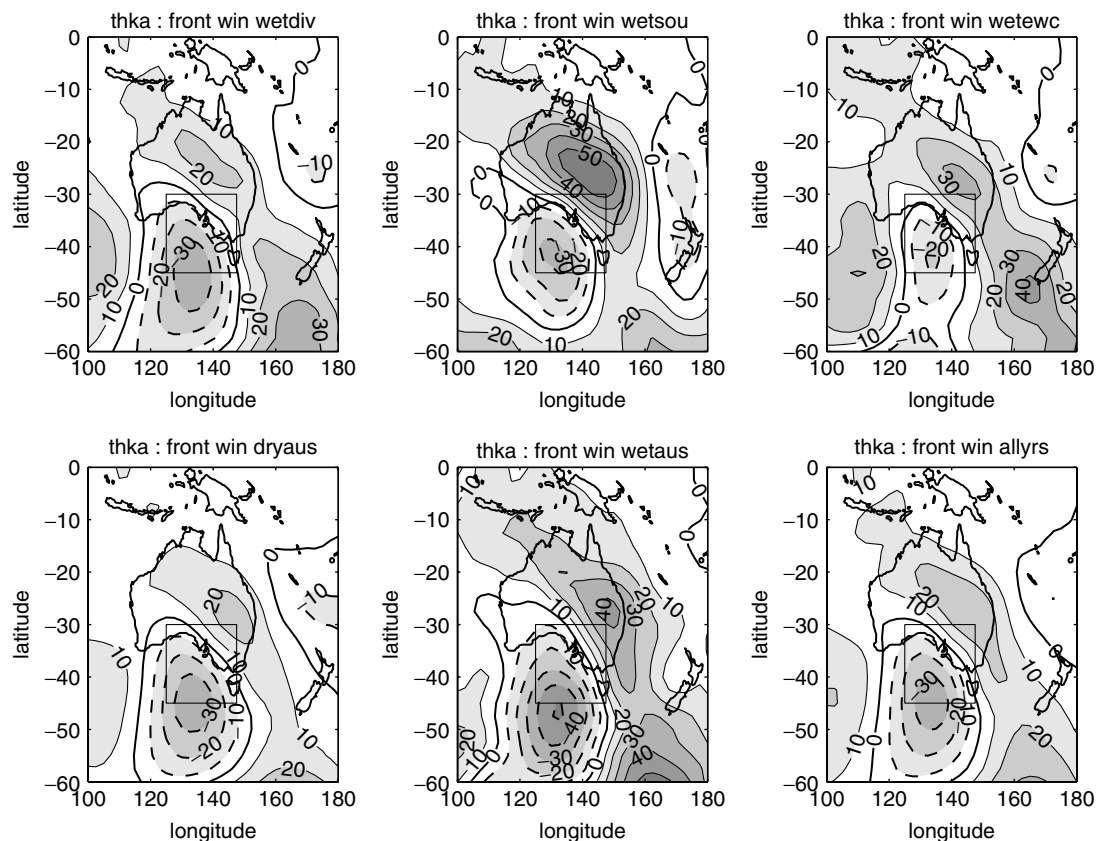


Figure 20. As in Figure 19, but for days on which frontal events occur.

strongly enhanced, with a large positive anomaly over northeastern continental Australia.

The mid-tropospheric flow pattern associated with each rainfall cluster grouping is quite distinct. We represent this flow by geopotential height anomalies at 500 hPa in Figure 21. For the rainfall patterns that are wettest in the Mallee ('wet south' and 'wet Australia'), the tropospheric flow is highly zonal with an annulus about the pole. This flow pattern is characteristic of the Southern Annular Mode (SAM) (Thompson and Solomon, 2002). Curiously, these two wet patterns are associated with SAM patterns of opposite sign in Figure 21. The 'wet south' pattern has lower than normal geopotential in the westerly belt and the 'wet Australia' pattern has higher than normal geopotential in this belt. The 'wet Australia' pattern is wet because the positive geopotential east of Australia is indicative of blocking there, which is more favorable to the development of cut-off low systems over Australia (Pook *et al.*, 2006). In Figure 18, we note that the 'wet Australia' pattern is dominated by cut-off rainfall in the Mallee. The years associated with this pattern have about twice the cut-off rainfall of other patterns. Conversely, the 'wet south' pattern is dominated by frontal rainfall, which is enhanced across the southern edge of the continent by the equatorward shift of the zonal westerlies indicated in Figure 21.

The jet stream fields associated with each rainfall pattern are not shown here for brevity. They show a strong influence of the subtropical jet. The location of

the jet maximum of the subtropical jet shifts from pattern to pattern, with the maximum located proximate to the region which is wet, or east of the continent for the 'dry Australia' pattern. The 'dry Australia' pattern is associated with unusually low-blocking activity in the Tasman Sea as indicated by the negative geopotential anomaly in this region in Figure 21 and a much weaker than normal region of anticyclonic vorticity (not shown). The reduction in blocking here reduces the incidence of cut-off lows in the analysis region (Section 4.3 and Pook *et al.* (2006)), and thus the amount of rainfall from cut-offs (Figure 18).

6. ENSO/IOD classification

In the previous section, we looked at variation in synoptic structure as a function of variation in interannual rainfall patterns. In this section, we keep the interannual focus, but instead of conditioning results by continental rainfall, we condition by the leading modes of variability of the Indian and Pacific Oceans. Rainfall in the Australian region is strongly influenced by both the El Niño/Southern Oscillation (ENSO) (Allan, 1988; Nicholls *et al.*, 1997; Wang and Hendon, 2007) in the Pacific Ocean and the IOD (Ashok *et al.*, 2003).

Meyers *et al.* (2007) have recently classified all years between 1885 and 1999 according to ENSO state (El Niño, neutral, La Niña) and IOD state (IOD+, neutral, IOD-). This classification defines a 3×3 matrix with

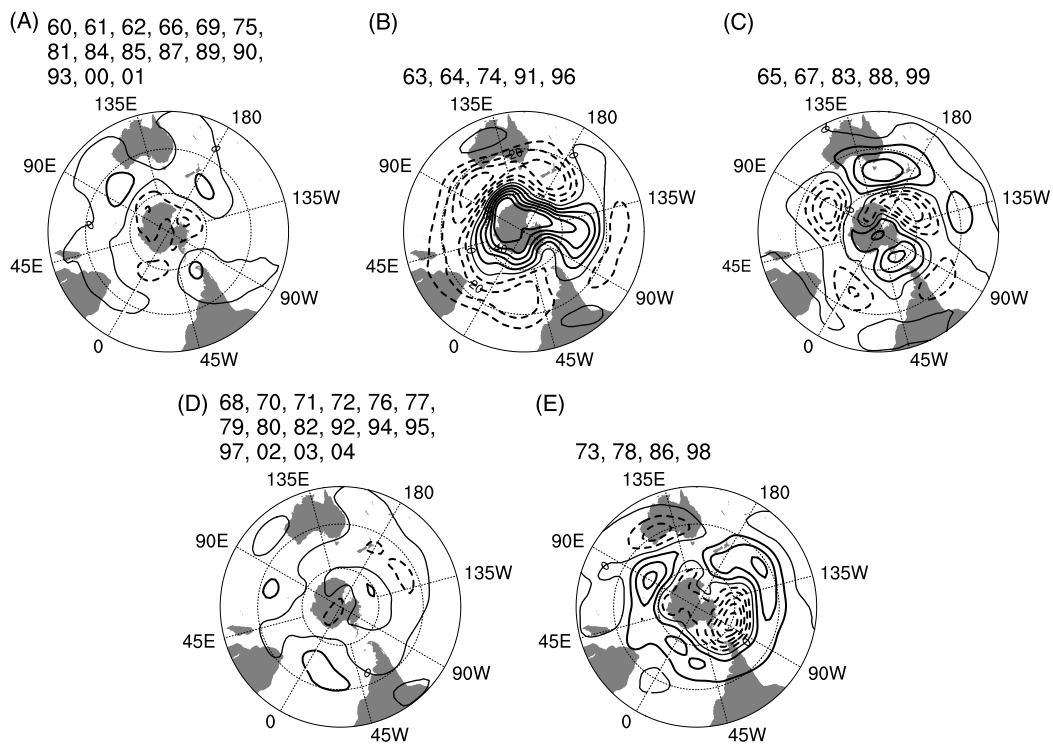


Figure 21. 500 hPa geopotential height anomaly patterns corresponding to the rainfall cluster years identified in Figure 17. The years comprising each pattern are listed above the pattern. The five cluster patterns from top left to bottom right are 'wet Divide' (A), 'wet south' (B), 'wet east/west coasts' (C), 'dry Australia' (D), and 'wet Australia' (E). Contour interval is 10 gpm. Negative contours are dashed.

years allocated to the appropriate cells of the matrix. In practice, the El Niño/IOD− and La Niña/IOD+ combinations seldom occur and so there are effectively only seven categories. For the southeast Australia region, wet years in this classification generally correspond to combinations in which IOD is negative, and/or there is a La Niña. Dry years generally correspond to combinations in which IOD is positive and/or there is an El Niño (Meyers *et al.*, 2007).

Thickness anomaly composites for the ENSO/IOD year groupings are shown in Figure 22 for the winter season. Both the El Niño and IOD+ composites (top row and right column in Figure 22) are marked by negative (cool) thickness anomalies over the Pacific Ocean east of Australia and in northeastern Australia. This is consistent with the cool sea surface temperature (SST) anomalies associated with this region for these categories (Meyers *et al.*, 2007). By contrast, the IOD− and La Niña categories (left column and bottom row in Figure 22) show warmer thickness anomalies in this region and warm anomalies northwest of Australia. These warm thickness anomalies are also consistent with the warm SST anomalies in these regions for IOD− and La Niña categories. Thickness anomalies do not mirror SST anomalies at any given point of time, as atmospheric thickness anomalies change more rapidly than oceanic SST anomalies. However, the atmosphere is thermally coupled to the ocean surface, and there does appear to be a relationship between SST and lower tropospheric temperature (thickness) over monthly and seasonal time scales, as exhibited by the corresponding anomaly patterns shown

here. This suggests a pathway via which SST anomalies may influence the development of synoptic systems: SST anomalies influence thickness anomalies, which in turn alters thickness gradients, thermal wind, and the potential for systems to develop. Similar relationships based on SST's and their gradients have been articulated in observational (Kushnir *et al.*, 2002) and modeling studies (Frederiksen and Balgovind, 1994; Kushnir *et al.*, 2002; Ummenhofer *et al.*, 2008).

The thickness field is partly set by thermal coupling and other time-mean processes, and partly via the passage of transient systems. When the thickness field in each ENSO/IOD category has the contribution from days in which each synoptic type occurs removed, the resulting patterns are similar to those in Figure 22. This suggests that these fields are reflective of a response to the background SST state. If the thickness anomaly fields in Figure 22 are viewed as background states for synoptic systems in these years, then the El Niño and IOD+ (see top row and right column in Figure 22) cold Pacific region thickness anomalies with warm anomalies to the south and west would tend to generate a thermal wind component that weakens the jet stream. Further, the cool SST/thickness background would weaken the positive (warm) thickness anomaly along the east coast that is characteristic of stronger cut-off systems in this region (Figure 8). The resulting reduction in the thickness gradient is associated with a reduction in rainfall. This is consistent with the reduction of rainfall in El Niño and IOD+ years. Conversely, for La Niña years (bottom row in Figure 22), the positive thickness anomaly over

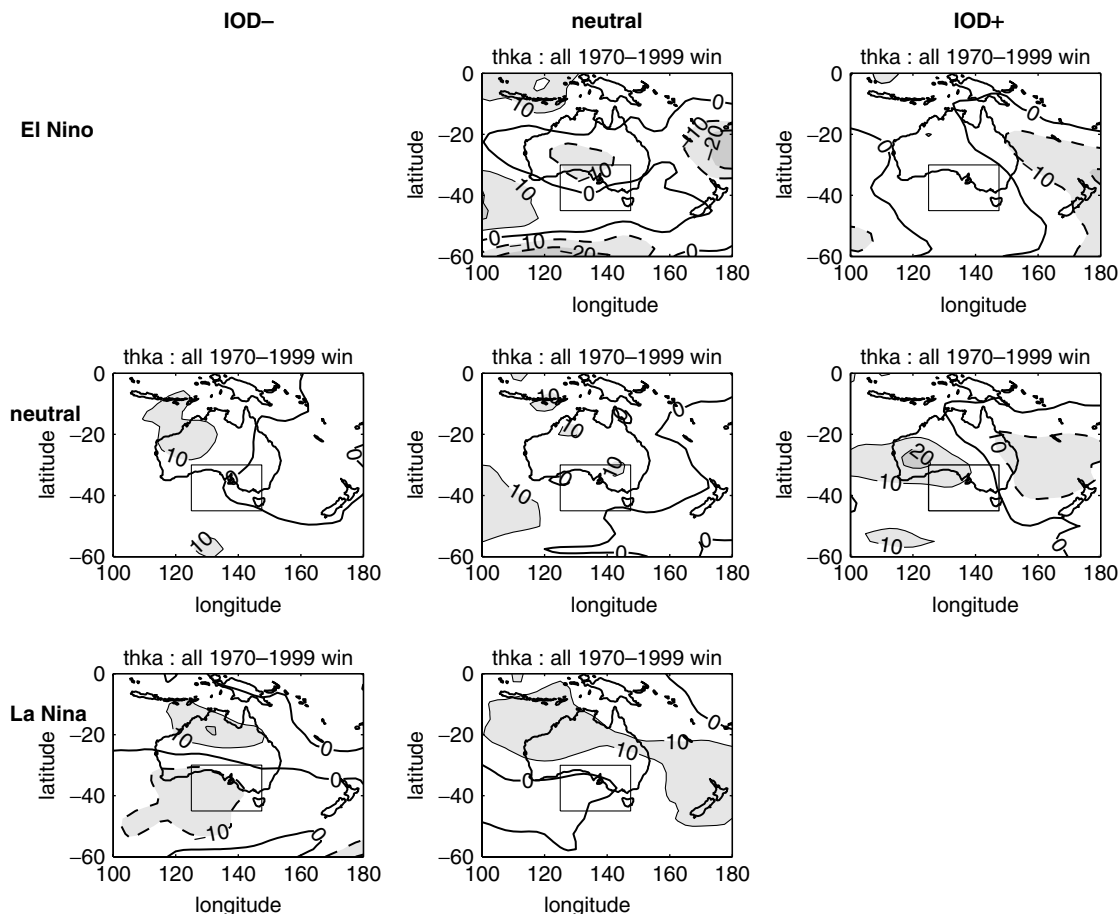


Figure 22. Thickness composite anomaly for ENSO/IOD categories for winter. The anomaly is calculated from the set of years 1970–1999. Only those years that fall into each ENSO/IOD category are used to calculate the composite anomaly. Units are in m. Dash contours indicate negative anomalies and solid contours indicate positive anomalies.

northern Australia and the Pacific Ocean, together with the negative thickness anomaly over southern Australia would result in an enhancement in thermal wind along the jet axis and a strengthening of the jet stream over southeastern Australia, along with an enhancement of thickness gradient for systems in this region. These features are consistent with the increase of rainfall in southeastern Australia in La Niña years.

Within each of the ENSO/IOD categories, we can also group the results according to the different synoptic categories. The thickness anomaly composites for cut-off systems in each of the ENSO/IOD categories are shown in Figure 23. Cut-offs have different signatures in the thickness pattern for different ENSO/IOD year groups, with the differences following the background thickness anomalies shown in Figure 22. Where the warm/cold anomalies are pronounced in Figure 22, the warm/cold anomaly is larger in Figure 23. Focusing on the region along the east coast of Australia, the ENSO/IOD category with a positive thickness anomaly in this region in Figure 22 (La Niña) exhibits an enhanced positive anomaly along the east coast and enhanced thickness gradient across the cut-off system in Figure 23. The ENSO/IOD categories with a negative thickness anomaly along the east coast in Figure 22 (El Niño, El

Niño/IOD+, IOD+) have only a weak positive thickness anomaly associated with the cut-off system in Figure 23. This weak positive anomaly is associated with a weak thickness gradient in the cut-off system and lower rainfall. The consistency of these relationships supports the notion that SST anomalies affect the strength of synoptic systems in the region.

The thickness anomaly pattern for cut-offs in La Niña categories shows a strong gradient across southeastern Australia, consistent with cut-off lows producing high rainfall. Composites of 250 hPa wind (jet stream) for cut-off days in each of the ENSO/IOD categories (not shown) show that the subtropical jet has a local maximum over southeastern Australia in the La Niña categories, whereas the maximum is located further east in the Pacific Ocean for El Niño and IOD+ categories, which is too far downstream to promote development of systems over southeastern Australia.

The thickness gradient for cut-offs between the continent and Pacific Ocean is not pronounced for the IOD-/ENSO-neutral category in Figure 23, yet that category is also favorable to cut-off rainfall. In this category, the Eady growth rate (not shown) shows a pronounced local maximum over the central southern portion of the Australian continent, consistent with an enhancement of

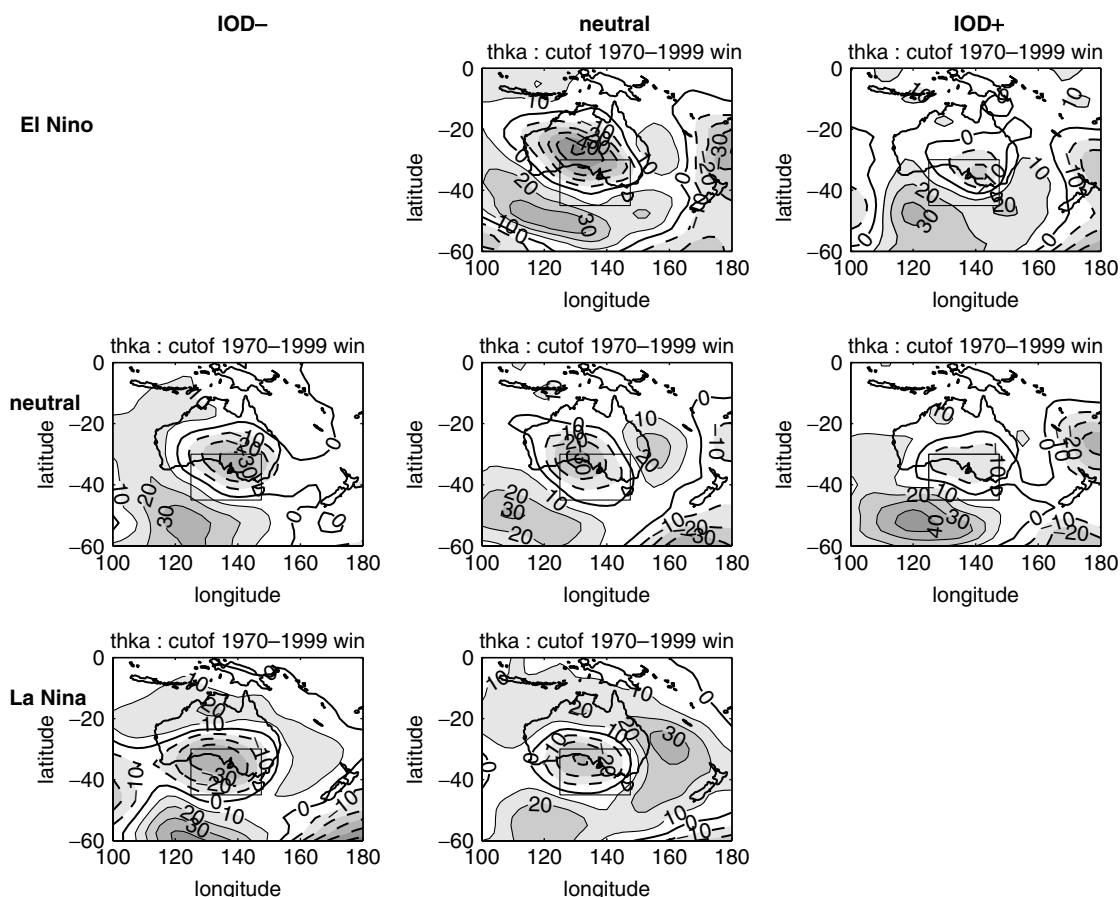


Figure 23. As in Figure 22, but the composite is only calculated on days for which cut-off low events occur. Units are in m.

the jet stream and thermal wind in this region. Those enhancements appear to be associated with the positive thickness anomaly northwest of Australia, which is proximate to the strong warm SST anomaly there in IOD– years.

For composites of frontal systems in the ENSO/IOD category years (not shown), the differences in thickness structure and other diagnostics from category to category are not very pronounced. Given that ENSO and IOD are the major tropical sources of interannual variability in the region, this suggests that frontal rainfall in the southeast is not strongly conditioned by tropical variability. On the other hand, we saw in Section 5 that frontal rainfall does vary in years where there is an equatorward extension of the westerlies exhibiting a SAM-like annular structure (Figure 21b). Thus, the midlatitudes appear to exert stronger direct control on frontal rain variability than the tropics. For cut-off systems, interannual variability is associated with tropical sources (ENSO/IOD) and also with extratropical sources. In Section 5, we saw that some years with high cut-off rainfall are associated with a SAM-like pattern that produces blocking in a region propitious for cut-off rainfall in Australia. These associations are just that however, and the mechanisms via which tropical and extratropical sources of variability influence cut-off and frontal rainfall in southeast Australia are not explored here. In the case of cut-off systems,

the controls on blocking need to be further understood (Pook and Gibson, 1999). Blocking in the Australian region is correlated with ENSO (tropical forcing) and is also intimately related to the long wave pattern, which is forced in substantial part via extratropical processes (thermal and orographic contrasts and transient eddies).

7. Conclusions

Rainfall in the Mallee region of southeastern Australia is highly variable on interannual time scales. One way to decompose that variability is to analyse the synoptic systems that produce the rainfall. Using a synoptic classification of frontal systems, cut-off lows, and other systems, much of the variability in cool season rainfall (April–October) is dominated by cut-off systems. Wet years in the southeast tend to be wet because there is enhanced rainfall from cut-off systems in those years.

The organization and structure of cut-off systems was shown to be distinct from frontal systems. Cut-off systems display a thermal cold pool cradled to the south by a warm thickness anomaly, which is indicative that the system has been ‘cut-off’ from the westerly stream. Both cut-off and frontal systems exhibit a strong increase in thickness gradient across the cold and warm pools as the rainfall associated with the system increases. The mechanisms via which these systems intensify appears to be

quite different though. Cut-off systems in the region grow in intensity in association with local increases in baroclinicity, vorticity, and a local increase in strength and cyclonic curvature of the subtropical jet. Frontal systems increase in intensity through an enhancement and confluence of both subtropical and polar jets. The baroclinic fields associated with intense fronts are less well localized than for cut-off systems and reflect the differing orientation of the jet systems. The vertical motion in cut-off systems is also more localized (relative to fronts) and displays the more classic comma wraparound of rising warm moist air and descending cold dry air.

In order to test variation of the synoptic types as a function of interannual rainfall variability, we analysed the dominant spatial patterns of rainfall across the Australian continent using a clustering algorithm. This yielded five robust pattern types. For the years associated with each pattern, we generated composites based on the days within each year that each synoptic type occurred. For the one pattern type (wet south) in which frontal rainfall predominates in the Mallee, the thickness gradient is enhanced in the frontal composite. Similarly, the thickness gradient is enhanced for composites of cut-offs where cut-off rainfall is enhanced, and the thickness gradient is diminished in dry years.

For the rainfall cluster patterns that are wettest in the Mallee region ('wet south' and 'wet Australia'), the hemispheric mid-tropospheric flow is highly zonal with an annulus about the pole indicative of the SAM. The 'wet south' pattern is indicative of the SAM- phase, while the 'wet Australia' pattern corresponds to the SAM+ phase. This suggests that different phases of the SAM can both be associated with enhanced rainfall in the Mallee region. The mechanisms are different in each case though. The 'wet south' pattern is largely the result of enhanced frontal rainfall, which is associated with the decreased pressure and enhanced equatorward westerly storm track in the SAM- phase. The 'wet Australia' pattern features a region of positive pressure anomalies and enhanced blocking southeast of Australia, which is favorable for the development of cut-off systems over southeastern Australia. This result illustrates that a flow pattern with a decreased or southward shift of the zonal mean storm tracks south of Australia is not necessarily detrimental to rainfall in Australia [cf. Karoly (2003); Frederiksen and Frederiksen (2007)]. In this case, the tendency for enhanced blocking promotes cut-off systems in the region that are very efficient at delivering rainfall to the Australian region. Thus, in projecting rainfall changes in the region, one needs to consider how any projected circulation changes will affect different synoptic types.

Interannual variability of rainfall and synoptic systems was also assessed for the modes of (tropical) oceanic variability most important for Australia; ENSO and IOD. When years are stratified according to ENSO and IOD states, the thickness anomaly patterns in the region reflect the underlying SST anomalies characteristic of each state. These thickness anomalies in turn are consistent with the enhancement of thickness gradients for cut-off systems in

La Niña and IOD- years and the reduction of thickness gradients for cut-off systems in El Niño and IOD+ years. Ocean SST anomalies along the Pacific coast and north of Australia are consistent with, and appear to influence, the intensity of thermal gradients of cut-off systems in southeast Australia, and thus also their rainfall. Frontal systems display less differentiation as a function of ENSO and IOD state. Variability in rainfall from frontal systems appears to be governed more so by extratropical processes than tropical processes, while cut-off systems display substantial variability which is associated with both tropical and extratropical sources.

In summary, rainfall variability in southeastern Australia can be described according to the kinds of synoptic classification used here. The predominant synoptic types have distinct signatures in the thermal field, in vertical motion, in concentration of baroclinic gradients, in vorticity, and in association with the major jet systems. Further, these indicators show consistent changes for the synoptic types as rainfall increases and in wet *versus* dry years. The changes in these features documented here do not explain the variability, but they help us to understand what it looks like. In order to explain the variability, we need to consider how these changes are related to broader circulation changes, and what the factors in turn are that govern these changes.

Acknowledgements

This work was funded by the CSIRO Climate Adaptation Flagship and the Managing Climate Variability Program of Land and Water Australia. CCU was supported by UNSW under a University International Postgraduate Award and by ARCNESS. Constructive comments and suggestions were provided by Michael Reeder and Steve Rintoul.

References

- Adams P, Horridge M, Madden J, Wittwer G. 2002. Drought, regions and the Australian economy between 2001–2 and 2004–5, Technical report, Monash University Centre of Policy Studies. General Paper G-135.
- Allan R. 1988. El Niño Southern Oscillation influences in the Australasian region. *Progress in Physical Geography* **12**(3): 313–348.
- Ashok K, Guan Z, Yamagata T. 2003. Influence of the Indian Ocean Dipole on the Australian winter rainfall. *Geophysical Research Letters* **30**(15): 1821–1824.
- Barry R, Carleton A. 2001. *Synoptic and Dynamic Climatology*. Routledge: London; 644.
- Bromwich D, Fogt R. 2004. Strong trends in the skill of the ERA-40 and NCEP-NCAR reanalyses in the high and midlatitudes of the southern hemisphere, 1958–2001. *Journal of Climate* **17**(23): 4603–4619.
- Cheng X, Wallace JM. 1993. Cluster analysis of the northern hemisphere wintertime 500-hPa height field: Spatial patterns. *Journal of the Atmospheric Sciences* **50**(16): 2674–2696.
- Frederiksen C, Balgovind R. 1994. The influence of the Indian Ocean/Indonesian SST gradient on the Australian winter rainfall and circulation in an atmospheric GCM. *Quarterly Journal of the Royal Meteorological Society* **120**: 923–952.
- Frederiksen J, Frederiksen C. 2007. Inter-decadal changes in Southern Hemisphere winter storm track modes. *Tellus* **59**(5): 599–617.

- Gallant A, Hennessy K, Risbey J. 2007. Trends in rainfall indices for six Australian regions: 1910–2005. *Australian Meteorological Magazine* **56**(4): 223–241.
- Griffiths M, Reeder M, Low D, Vincent R. 1998. Observations of a cut-off low over southern Australia. *Quarterly Journal of the Royal Meteorological Society* **124**(548): 1109–1132.
- Hirschberg P, Fritsch J. 1991. Tropopause undulations and the development of extratropical cyclones. Part I: Overview and observations from a cyclone event. *Monthly Weather Review* **119**(2): 496–517.
- Hoskins B, Valdez PJ. 1990. On the existence of storm tracks. *Journal of the Atmospheric Sciences* **47**: 1854–1864.
- Jeffrey S, Carter J, Moodie K, Beswick A. 2001. Using spatial interpolation to construct a comprehensive archive of Australian climate data. *Environmental Modelling & Software* **16**(4): 309–330.
- Kalnay E, Kanamitsu M, Kistler R, Collins W, Deaven D, Gandin L, Iredell M, Saha S, White G, Woollen J, Zhu Y, Leetmaa A, Reynolds R, Chelliah M, Ebisuzaki W, Higgins W, Janowiak J, Mo KC, Ropelewski C, Wang J, Roy Jenne, Dennis Joseph. 1996. The NCEP-NCAR 40-year reanalysis project. *Bulletin of the American Meteorological Society* **77**: 437–471.
- Karoly D. 2003. Ozone and climate change. *Science* **302**: 236–237.
- Keyser D, Shapiro M. 1986. A review of the structure and dynamics of upper-level frontal zones. *Monthly Weather Review* **114**(2): 452–499.
- Kushnir Y, Robinson W, Bladé I, Hall N, Peng S, Sutton R. 2002. Atmospheric GCM response to extratropical SST anomalies: synthesis and evaluation. *Journal of Climate* **15**: 2233–2256.
- Lavery B, Joung G, Nicholls N. 1997. An extended high quality historical rainfall data set for Australia. *Australian Meteorological Magazine* **46**: 27–38.
- McIntosh P, Pook M, Risbey J, Lisson S, Rebbeck M. 2007. Seasonal climate forecasts for agriculture: towards better understanding and value. *Field Crops Research* **104**(1–3): 130–138.
- Meyers G, McIntosh P, Pigot L, Pook M. 2007. The years of El Niño, La Niña, and interactions with the tropical Indian Ocean. *Journal of Climate* **20**(13): 2872–2880.
- Nicholls N. 1997. Increased Australian wheat yield due to recent climate trends. *Nature* **387**: 484–485.
- Nicholls N, Drosowsky W, Lavery B. 1997. Australian rainfall variability and change. *Weather* **52**(3): 66–71.
- Paciorek C, Risbey J, Ventura V, Rosen R. 2002. Multiple indices of northern hemisphere cyclone activity, winters 1949–99. *Journal of Climate* **15**(13): 1573–1590.
- Petterssen S. 1955. A general survey of factors influencing development at sea level. *Journal of Meteorology* **12**(1): 36–42.
- Philander S. 1985. El Niño and La Niña. *Journal of the Atmospheric Sciences* **42**(23): 2652–2662.
- Pook M, Gibson T. 1999. Atmospheric blocking and storm tracks during SOP-1 of the FROST project. *Australian Meteorological Magazine* **48**: 51–60, Special Edition.
- Pook M, McIntosh P, Meyers G. 2006. The synoptic decomposition of cool-season rainfall in the southeastern Australian cropping region. *Journal of Applied Meteorology and Climatology* **45**(8): 1156–1170.
- Saji N, Goswami B, Vinayachandran P, Yamagata T. 1999. A dipole mode in the tropical Indian Ocean. *Nature* **401**(6751): 360–363.
- Sutcliffe R, Forsdyke A. 1950. Use of upper air thickness patterns in forecasting. *Quarterly Journal of the Royal Meteorological Society* **76**(328): 189–217.
- Thompson D, Solomon S. 2002. Interpretation of recent southern hemisphere climate change. *Science* **296**: 895–899.
- Thorncroft C, Hoskins B, McIntyre M. 1993. Two paradigms of baroclinic-wave life-cycle behaviour. *Quarterly Journal of the Royal Meteorological Society* **119**(509): 17–55.
- Trenberth K, Mo K. 1985. Blocking in the Southern Hemisphere. *Monthly Weather Review* **113**(1): 3–21.
- Ummenhofer C, Gupta A, Pook M, England M. 2008. Anomalous rainfall over southwest Western Australia forced by Indian Ocean sea surface temperatures. *Journal of Climate* **21**: 5113–5134.
- Wang G, Hendon H. 2007. Sensitivity of Australian rainfall to inter-El Niño variations. *Journal of Climate* **20**: 4211–4226.
- Ward J. 1963. Hierarchical grouping to optimize an objective function. *Journal of the American Statistical Association* **58**(301): 236–244.
- Watkins A, Trewin B. 2007. Australian climate summary: 2006. *Bulletin of the Australian Meteorological and Oceanographic Society* **20**(1): 10–17.